Am J Transl Res 2026;18(1):248-264
www.ajtr.org /ISSN:1943-8141/AJTR0165248

Original Article

Modified constraint-induced movement therapy improves functional recovery after ischemic stroke and its impacts on exosome-derived microRNAs

Beiyao Gao[1*], Ruidong Ge[1*], Ying Xing[2], Peile Liu[3], Shan Jiang[1]

[1]Department of Rehabilitation Medicine, China-Japan Friendship Hospital, Beijing, China; [2]Department of Rehabilitation, Zhongshan Hospital, Fudan University, Shanghai, China; [3]Department of Rehabilitation, Fujian Medical University Union Hospital, Fuzhou, Fujian, China. [*]Equal contributors.

Received April 11, 2025; Accepted December 8, 2025; Epub January 15, 2026; Published January 30, 2026

Abstract: Objective: To investigate whether modified constraint-induced movement therapy (mCIMT) improves brain function after stroke by increasing the concentrations of exosomes and microRNA. Methods: Blood samples from 16 stroke patients (mCIMT group N=8, control group N=8) were analyzed for cytokines and exosomal microRNAs. Data from electronic medical records and clinical outcomes were also correlated. For the animal model, SD rats underwent middle cerebral artery occlusion (MCAO). The mCIMT group received 2 hours of daily intensive limb training for 14 days, starting 7 days post-MCAO, while the control group was untreated. Exosomes were extracted from brain tissue on day 21, followed by nanoparticle tracking and microRNA sequencing. Exosomes from both groups, as well as a vehicle, were injected into the lateral ventricles of MCAO rats, and they were named the Exo-mCIMT group, Exo-control group and vehicle group. Behavioral tests and histopathological staining were performed on day 21 among the three groups. Results: mCIMT significantly increased exosome content in the plasma of stroke patients, with exosome size correlated with the Fugl-Meyer Motor Function Assessment (FMA-UE, R^2=0.428). In rats, the mCIMT group had a higher concentration of exosomes in brain tissue (3.73e+10 particles/ml) compared to the control group (0.95e+10 particles/ml, P=0.0030). MicroRNA sequencing revealed distinct expression profiles between the groups. Furthermore, the exo-mCIMT group exhibited significantly higher levels of MAP2 and VEGF expression, along with notable improvements in neurobehavioral outcomes. Conclusion: These findings suggest that mCIMT promotes neural recovery through increased exosome and microRNA activity in the brain, which plays an important role in neuronal activity after brain injury.

Keywords: Cerebral ischaemic injury, stroke, rehabilitation, mCIMT, exosomes

Introduction

Stroke is a leading cause of chronic disability in adults, and active rehabilitation can increase patients' independence in daily life. Among the rehabilitation techniques used for stroke patients, CIMT/mCIMT is recommended frequently and supported by substantial evidence, and it has demonstrated significant clinical value and experienced rapid clinical adoption worldwide in recent years [1-3]. CIMT/mCIMT involves restricting the use of the nonaffected upper limb while the patient is awake and engaging the affected upper limb in task-intensive exercises. Traditional CIMT requires patients to wear a device such as a sling, splint, or glove to immobilize the nonaffected limb for 90% of their waking hours. To minimize the adverse effects of excessive restriction, a modified version of this therapy, known as modified Constraint-Induced Movement Therapy (mCIMT), has been introduced in recent years. mCIMT involves rational adjustments to the intensity and duration of both restriction and intensive training. Moreover, several meta-analyses have demonstrated that mCIMT is a feasible and effective technique for rehabilitation [4-6].

During the poststroke period, the two cerebral hemispheres exhibit different patterns of brain

https://doi.org/10.62347/YBJF9113

activity; CIMT/mCIMT can alter these patterns, promoting neural plasticity accompanied by the upregulation of synaptic markers [7, 8]. Recent clinical studies have shown that CIMT/mCIMT-can influence brain neural plasticity [9], potentially through the expression of neurotrophic and repair-related factors secreted by various cells [10-18]. While neuronal plasticity is intrinsically linked to the complex structure and function of the CNS, little is known about the intercellular communication changes induced by mCIMT following cerebral ischaemic injury.

Various cells within the CNS release extracellular vesicles (EVs) into the microenvironment under physiological or pathological conditions. These vesicles, ranging from 50 to 150 nm in diameter, contain proteins, glycoproteins, lipids, and nucleic acids, including RNA, which serve as biological clues for EV targeting and cellular interactions [19-21]. RNAs, particularly noncoding small RNA molecules such as microRNAs (miRNAs), act as negative regulators by inducing mRNA degradation or inhibiting mRNA translation, thereby modulating gene expression post-transcriptionally and influencing crucial biological processes such as cell development, proliferation, differentiation, and apoptosis. The contents of EVs, including microRNAs, have been used for prognostic prediction, diagnosis, monitoring, and treatment in patients with neurological injuries, with potential clinical applications as disease biomarkers [22-24]. Moreover, preclinical studies of stroke patients suggest that EVs derived from transplanted stem cells may contribute to neurorepair mechanisms [25-27].

Research has shown that during early cerebral ischaemia in rats subjected to MCAO, plasma levels of EVs increase, whereas EVs in brain tissue do not exhibit a similar increase in concentration [28]. Injection of EVs secreted by mesenchymal stem cells has been found to protect neuro-injury and functional recovery in rats' post-stroke, demonstrating protective effects on neuronal injury [29-31]. Consequently, this study focuses on whether mCIMT influences brain neuroprotection through the upregulation of EVs, and on the characterization of the microRNAs contained within EVs. It further emphasizes the translation of crucial RNA findings from basic science into clinical validation in stroke patients. The investigation aims to determine whether mCIMT modifies the concentration or molecular cargo of EVs, which act as mediators of intercellular communication, and to clarify the role of EVs in promoting neuroprotection during cerebral ischaemic injury.

Materials and methods

Patients

This analysis included 16 stroke patients, 8 of whom received modified constraint-induced movement therapy (mCIMT), while 8 served as the control group. All patients were treated at the Rehabilitation Medicine Department of the China-Japan Friendship Hospital between 2020 and 2023. The study was approved by the Ethics Committee in China (Approval No. 2023-KY-067). The clinical trial registration number is ChiCTR2300074165, and the details can be accessed at [https://www.chictr.org.cn/showproj.html?proj=198903].

Patients were included if they: (1) met the diagnostic and classification criteria for stroke established by the Fourth National Cerebrovascular Disease Conference; (2) had cerebral infarction or hemorrhage confirmed by CT or MRI; (3) were conscious with stable vital signs; (4) were within 2 weeks to 6 months post-onset; (5) were aged ≥18 years; (6) exhibited active wrist dorsiflexion of at least 10° on the affected side, with at least two other fingers (excluding the thumb) capable of 10° dorsiflexion, and had a modified Ashworth score of ≤1+ in the upper extremity; and (7) were capable of independent walking.

Patients were excluded if they: (1) had unstable medical conditions; (2) presented with moderate to severe cognitive impairment (MMSE score ≤24); (3) had other neurological disorders affecting upper limb function; (4) exhibited severe upper limb spasticity (Ashworth score >2); or (5) reported severe pain (VAS score ≥7).

Participants were withdrawn from the study if: (1) they requested to revoke informed consent; or (2) the investigator determined that discontinuation was medically necessary.

Patients in the mCIMT group wore inhibitory gloves to restrict the unaffected hand and performed specific behavioral retraining and intensive repetitive exercises with the affected hand.

This was supplemented by targeted and selective motor imagery training. One-on-one training was provided under the guidance of an occupational therapist, including 2-3 selected shaping tasks for the patient with intensive training lasting 20 minutes, twice per week. Additionally, daily at-home restriction of the unaffected hand was implemented for 2 hours. Duration of therapy was 4 weeks. Patients in the control group did not wear inhibitory gloves, and their unaffected hand was not restricted. All other training components were identical to those of the intervention group. Clinical parameters, including demographic data, cytokine levels, and pre- and post-treatment FMA-UE scores and Barthel Index at admission, were recorded from the patients' electronic medical records.

Patients' plasma

Plasma exosomes were analyzed in this study. Blood samples were collected after 4 weeks of mCIMT intervention and upon patient admission to the Rehabilitation Medicine Department. Processing was initiated within 1 hour. To isolate plasma, blood samples were centrifuged at 1,900 × g for 10 minutes at 4°C via a swinging bucket rotor. The supernatant (plasma) was carefully collected and stored at -80°C. To isolate EVs, thawed plasma supernatant was sequentially centrifuged at 300 × g for 10 minutes, 3,000 × g for 20 minutes, 10,000 × g for 30 minutes, and 100,000 × g for 2 hours at 4°C. The EVs were stored at -80°C to prevent degradation.

Experimental animals

The animals were obtained from Shanghai SIPPR-BK LAB Animal Co., Ltd. (Licence No. SCXK (Hu) 2018-0006) and included male Sprague-Dawley rats weighing 250-300 g, aged 7-9 weeks. This work remained in line with the ARRIVE 2.0 guidelines. The experimental animals were housed in a clean (specific pathogen-free-grade) animal facility in the Fudan University Laboratory Animal Science Department (national SPF level), with four rats per cage, having free access to food and water, while being maintained at a temperature of 23±1°C with a 12-hour light-dark cycle (lights off at 8 PM and on at 8 AM). Eighteen rats were randomly assigned to the mCIMT group (N=9) or the control group (N=9). At 21 days post-MCAO surgery, the brain tissues were collected from each rat. The animal experiments were approved by the Institutional Animal Care and Use Committee of Fudan University, under approval number 201802173S.

MCAO model

The rats were anaesthetized with 10% chloral hydrate and maintained at a rectal temperature of approximately 36.5°C. MCAO was induced in the MCAO group by inserting a poly-L-lysine-coated suture into the left middle cerebral artery, which was withdrawn after 90 minutes to induce ischaemia. Laser Doppler flowmetry was used to monitor cerebral blood flow in the territory of the middle cerebral artery before and after suture insertion. Neurological deficits were assessed using a 0-4 point scale upon awakening from anaesthesia; rats scoring 0 or 4 points were excluded from the study.

Modified constraint-induced movement therapy (mCIMT)

In mCIMT, the unaffected limb (left forelimb) was restrained against the chest using a bandage for 2 hours daily. Starting from the 7th day post-MCAO, mCIMT was maintained for 2 weeks. Training was conducted using a custom-built wheel device (Chinese patent No. 201008862247.8). On the first day, training involved continuous movement at 2 revolutions per minute (r/min) for 10 minutes, increasing to 20 minutes at the same speed on the second day, and starting from the third day, training continued at 4 r/min for 20 minutes. Training was paused during behavioural testing. Before the first training session, the rats were acclimatized to the device for 20 minutes. The control group underwent a similar training regimen but without restriction of the unaffected limb.

Extraction of extracellular vesicles from brain tissues

We performed euthanasia by intraperitoneal injection of an overdose of sodium pentobarbital (150 mg/kg), followed by confirmation of death via absence of pedal reflex and cessation of heartbeat. This method complies with the AVMA Guidelines for the Euthanasia of Animals and was approved by our Institutional Animal Care and Use Committee. The brain tissues were collected 21 days after MCAO. To

isolate EVs from brain tissue, fresh or frozen brain hemispheres were incubated in Hibernate-E solution containing 20 U/mL papain at 37°C for 15 minutes. Digestion was terminated by adding pre-chilled Hibernate-E. Exosome extraction followed previously described protocols [32, 33]. Briefly, the tissue was gently homogenized on ice, filtered sequentially through 40-μm and 0.2-μm filters, and the filtrate was collected. The filtrate was centrifuged at 3,000 g for 10 minutes at 4°C to remove debris, and the supernatant was further centrifuged at 10,000 g for 20 minutes at 4°C to eliminate impurities. For EV precipitation, the supernatant was mixed with Exosome Concentration Solution (ECS) in a 1:5:1 ratio with PBS, vortexed, incubated at 2-8°C for 2 hours, and centrifuged at 10,000 g for 60 minutes at 4°C to pellet exosomes. The pellet was resuspended in 100 μL PBS. In parallel, sequential ultracentrifugation steps were performed on thawed supernatant (300 × g for 10 min, 3,000 × g for 20 min, 10,000 × g for 30 min, and 100,000 × g for 2 h at 4°C) to ensure EV enrichment. The final EV pellet was stored at -80°C to prevent degradation. To minimize variability across animals, all samples were processed under identical experimental conditions, using the same isolation protocol, buffer system, and instrument calibration settings. EV concentrations were expressed relative to initial sample volume and measured under standardized dilution, which allowed for consistent comparisons across groups.

Qualitative and quantitative analysis of EVs

Electron microscopy: EVs extracted from CSF and plasma were subjected to negative staining with uranyl acetate and lead citrate and applied onto copper grids. Excess liquid was blotted away with filter paper and air-dried at room temperature. Transmission electron microscopy was used to visualize EV morphology.

Nanoparticle tracking analysis (NTA): NTA was employed to assess EV size distribution and concentration. This method tracks the Brownian motion of individual particles and calculates hydrodynamic diameter and particle concentration based on the Stokes-Einstein equation. The sample chambers were rinsed with deionized water and calibrated with 110-nm polystyrene microspheres. EV samples isolated from CSF and plasma were diluted in 1× PBS (Biological Industries, Israel) and analyzed in triplicate for reproducibility.

Transcriptome sequencing

RNA extraction, microRNA-seq library construction, and high-throughput sequencing using Illumina HiSeq were performed by a second-generation sequencing company (Shanghai Majorbio Biopharm Technology Co., Ltd.). The reads were postprocessed via decoding indices to recover individual samples. Adapter sequences were trimmed, and sequences containing "N" or aligning with ribosomal DNA repeat units (GenBank accession number HSU13369) were excluded. The resulting products were purified, fragmented, and subjected to quality control to obtain the final libraries, followed by sequencing on the Illumina HiSeq platform.

Stereotaxic coordinates for lateral ventricular injection

Secure the rat in a stereotaxic frame, Disinfect the scalp, make a midline incision to expose the skull, and identify the bregma and lambda to confirm proper alignment. Using a magnifying tool, locate the injection site based on the coordinates and drill a small hole through the skull. Stereotaxic injection into the lateral ventricles of the rat brain is guided by standard brain atlases. The coordinates for targeting the lateral ventricles relative to the bregma, are: Anterior-Posterior (AP): -0.8 mm (posterior to bregma); Medial-Lateral (ML): ±1.5 mm (lateral to the midline); Dorsal-Ventral (DV): -3.5 mm (ventral from the skull surface). Insert the hamilton syringe into the target site. Slowly inject the exosome solution (2 μL) at a controlled rate at 0.2 μL/min. Allow the needle or cannula to remain in place for 5 minutes to ensure proper diffusion of the exosomes. Carefully withdraw the needle and close the incision.

Catwalk gait analysis

Gait was evaluated via the CatWalk® 7.1 digital gait analysis system. This system consists of a 130 cm long glass runway parallel to internally illuminated components. For each rat (N=6 per group), data were recorded only when all four paws completed at least three passes across the glass runway. CatWalk® 7.1 software was used to analyse gait-related parameters, such

as the contact intensity of the forelimbs and hindlimbs, which reflect the limb ground reaction force and gait speed. The rats were allowed to acclimate to the apparatus three days prior to MCAO. The day of MCAO was considered day 1, and gait analysis was performed on T1 (days 14), and T2 (days 21) post-MCAO. The experimenter and data analyst were blinded to the group assignments.

Tissue extraction and immunofluorescence staining

Euthanize the rat following established ethical guidelines. Carefully dissect the brain and rinse it with cold PBS to remove blood and debris. Fix the brain in 4% paraformaldehyde (PFA) in PBS at 4°C for 4 hours. After fixation, transfer the brain to a cryoprotectant solution and store it at 4°C until sectioning. Embed the fixed brain in OCT compound, freeze it on dry ice, and section it into 20 μm coronal slices using a cryostat or microtome. Mount the sections on glass slides and store them at -80°C until further use. Before staining, allow the sections to equilibrate to room temperature. Permeabilize the tissue with 0.1% Triton X-100 in PBS for 10 minutes, then block non-specific binding by incubating the sections in a blocking solution for 1 hour at room temperature. Apply the primary antibodies diluted in blocking solution as follows: Anti-VEGF (1:100), Anti-MAP2 (1:200), TUNEL reaction mixture (according to kit instructions), and Anti-GFAP (1:300). Incubate the sections overnight at 4°C. The next day, wash the sections three times with PBS for 5 minutes each to remove unbound primary antibodies. Add secondary antibodies (diluted 1:500 in blocking solution) and incubate for 1 hour at room temperature. Wash again three times with PBS for 5 minutes each to remove unbound secondary antibodies. Counterstain nuclei using DAPI-containing mounting medium, then visualize the stained sections using a fluorescence or confocal microscope. Capture images and analyze fluorescence intensity to quantify VEGF, MAP2, TUNEL-positive cells, and GFAP expression levels.

Sample size

The sample size was theoretically estimated based on the between-group differences in the primary endpoints (relative expression of exosomal miRNAs/EV concentration), using a two-independent-sample t-test formula, with a significance level of $\alpha=0.05$ (two-sided) and a target power of 80%. According to Cohen's d, a large effect size ($d=0.8$) would require approximately 25 participants per group, while a medium effect size ($d=0.5$) would require about 63 participants per group. Given the exploratory nature of this study and the limited number of eligible participants, a total of 16 subjects were ultimately included (mCIMT group: n=8; control group: n=8), primarily to estimate effect sizes and variance for the design of subsequent confirmatory studies.

Statistical analysis

All the experimental data were statistically analysed using GraphPad Prism 7.0 and SPSS 20.0 software. In this study, the sample size was determined using statistical power analysis based on expected effect size, standard deviation, significance level, and desired power. Continuous variables are presented as the means ± standard deviations (means ± SD). Randomization of the subjects into treatment groups was performed using a computer-based method accessible from GraphPad (GraphPad's Randomization Calculator; https://www.graphpad.com/quickcalcs/randomize1). Normality testing of continuous variables was performed using the Shapiro-Wilk test. For normally distributed data with equal variances, comparisons between two groups were conducted using the independent-samples *t* test. For non-normally distributed data or data with unequal variances, the Mann-Whitney U test was applied. Correlations between FMA-UE score changes and exosome diameters were evaluated using Spearman's rank correlation coefficient, which is appropriate for non-parametric correlation analysis. A P value of less than 0.05 was considered to indicate statistical significance. For microRNA sequencing data, differential expression analysis was performed using the DESeq2 package, which applies a negative binomial distribution model to estimate variance-mean dependence in count data. To control for multiple testing, the Bonferroni correction was applied, and adjusted P values <0.05 were considered statistically significant.

Group allocation and blinding

Randomization and blinding were implemented at key stages of the experiment (group alloca-

Table 1. Clinical parameters of stroke patients in mCIMT group and control groups

	mCIMT (N=8)	con (N=8)	χ^2 value	t value	*P* value
Male	75%	87.50%	.410		0.522
Post Stroke Duration (days)	90±45	54±45		1.568	0.139
Age	63±9	59±13			0.45
HP	75%	75%	.000		1
DM	50%	25%	1.067		0.302
CVD	12.50%	25%	.410		0.522
Smoke	50%	62.50%	.254		0.614
Barthel index-baseline	79±12	80±13		-.196	0.848
FMA-UE-baseline	49±7	49±4		-1.700	0.896

FMA-UE: Fugl-Meyer Motor Function Assessment Upper Extremity, DM: Type 2 diabetes mellitus, CVD: cardiovascular disease, HP: hypertension.

Table 2. The inflammatory cytokines in serum of stroke patients between the mCIMT group and control group

	mCIMT (N=8)	con (N=8)	t value	*P* value
IL-6	45.123±58.606	29.953±36.003	0.624	0.543
IL-1	11.695±7.441	12.162±8.508	-0.117	0.909
IL-10	1.162±0.267	1.088±0.242	0.587	0.567
IL-4	2.104±0.422	2.077±0.632	0.101	0.921
TNF-a	16.222±10.997	16.628±13.496	-0.066	0.948

Table 3. Fugl-Meyer motor function assessment of stroke patients

	mCIMT (N=8)	con (N=8)	T value	*P* value
FMA-UE-baseline	47	51	-1.700	0.111
FMA-UE-post therapy	55	55	0.204	0.842
FMA-UE-change	9	4	2.528	0.024

tion, treatment, and outcome assessment) to reduce bias and ensure the reliability and reproducibility of the findings. Blinding was maintained as long as possible, with unblinding only occurring after data collection and analysis were completed.

Results

Exosomal microRNA-126-3p of ischaemic stroke patients

The baseline characteristics of the mCIMT and control patient groups, including age, sex, smoking history, stroke complications, and other clinical data, showed no significant differences (**Table 1**). Similarly, there were no significant differences in several key inflammatory cytokines in serum between the groups (**Table 2**). Our observation that the change in FMA-UE scores indicates mCIMT was more effective than the control group aligns with the benefits often associated with mCIMT (P=0.024) (**Table 3**).

The concentration and diameter of exosomes were analysed by nanoparticle tracking analysis (NTA), which has been recognized as a method for characterizing exosomes. The principle of this method involves tracking and analysing the Brownian motion of each particle and calculating the hydrodynamic diameter and concentration of the nanoparticles using the Stokes-Einstein equation. A comparison of the exosome concentration in the plasma between the two groups (measured in particles/ml) revealed that the relative concentration was high in both patient groups (**Figure 1A** and **1B**). Moreover, the mCIMT group presented with a significantly greater concentration of exosomes than did the control group (P=0.0189). The mean values for the control and mCIMT groups were 2.57e+10 particles/ml and 6.13e+9 particles/ml, respectively (**Figure 1C**). Importantly, the exosome diameters in the mCIMT group were significantly higher than those in the control group (P=0.0162, **Figure 1D**). Additionally, the improvement in FMA-UE scores after treatment was significantly greater in the mCIMT group compared to the control group (P=0.0241, **Figure 1E**). Surprisingly, we also found that exosome diameter levels were correlated with upper limb motor function recovery (R^2=0.428, P=0.006. **Figure 1F**).

mCIMT increases the concentration of exosomes in the brain tissue of rats with cerebral ischaemic injury

Twenty-one days after MCAO, we collected the brain tissues, extracted exosomes and compared the concentration of exosomes in the

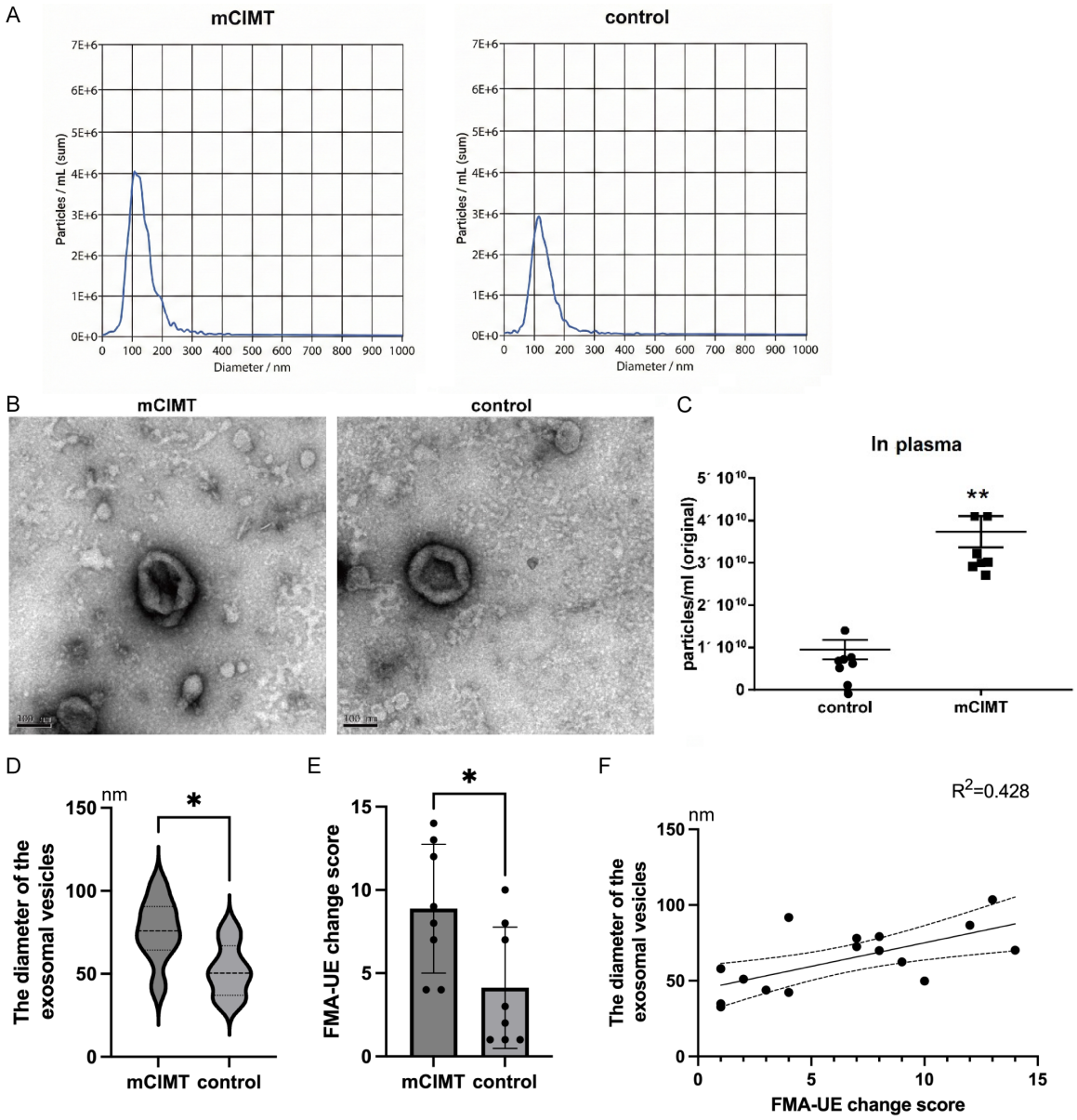

Figure 1. mCIMT increases the concentration of exosomes in the plasma of stroke patients. A. NTA reveals the peak size and peak area ratio. The size of exosomes is generally in the range of 30-200 nm. B. Ultrastructure of the exosomes observed via transmission electron microscopy (80000×). Scale bar=100 nm. C. Content of exosomes in the plasma of mCIMT and control groups. D. Diameter of exosomes in the plasma of mCIMT and control groups. E. Fugl-Meyer Assessment of Upper Extremity (FM-UE) change score of mCIMT and control groups after intervention. F. The correlation between FMA-UE change score and diameter of exosomes in the stroke patients. N=8 patients/group, *P<0.05, **P<0.01.

brain between the two groups (unit: particles/ml) (**Figure 2A** and **2B**). The results revealed that the relative concentration was high in both groups, and the content in the mCIMT group was significantly greater than that in the control group (P=0.0030). The relative values for the control and mCIMT groups were 0.95e+10 particles/ml and 3.73e+10 particles/ml, respectively (**Figure 2C**). In mCIMT, the unaffected limb (left forelimb) was restrained against the chest, as shown in **Figure 2D**.

Brain exosomal microRNA Levels from the mCIMT group and control group

The levels of microRNAs in the brain tissue exosomes of both groups were evaluated by microRNAs sequencing identification (**Table 4**).

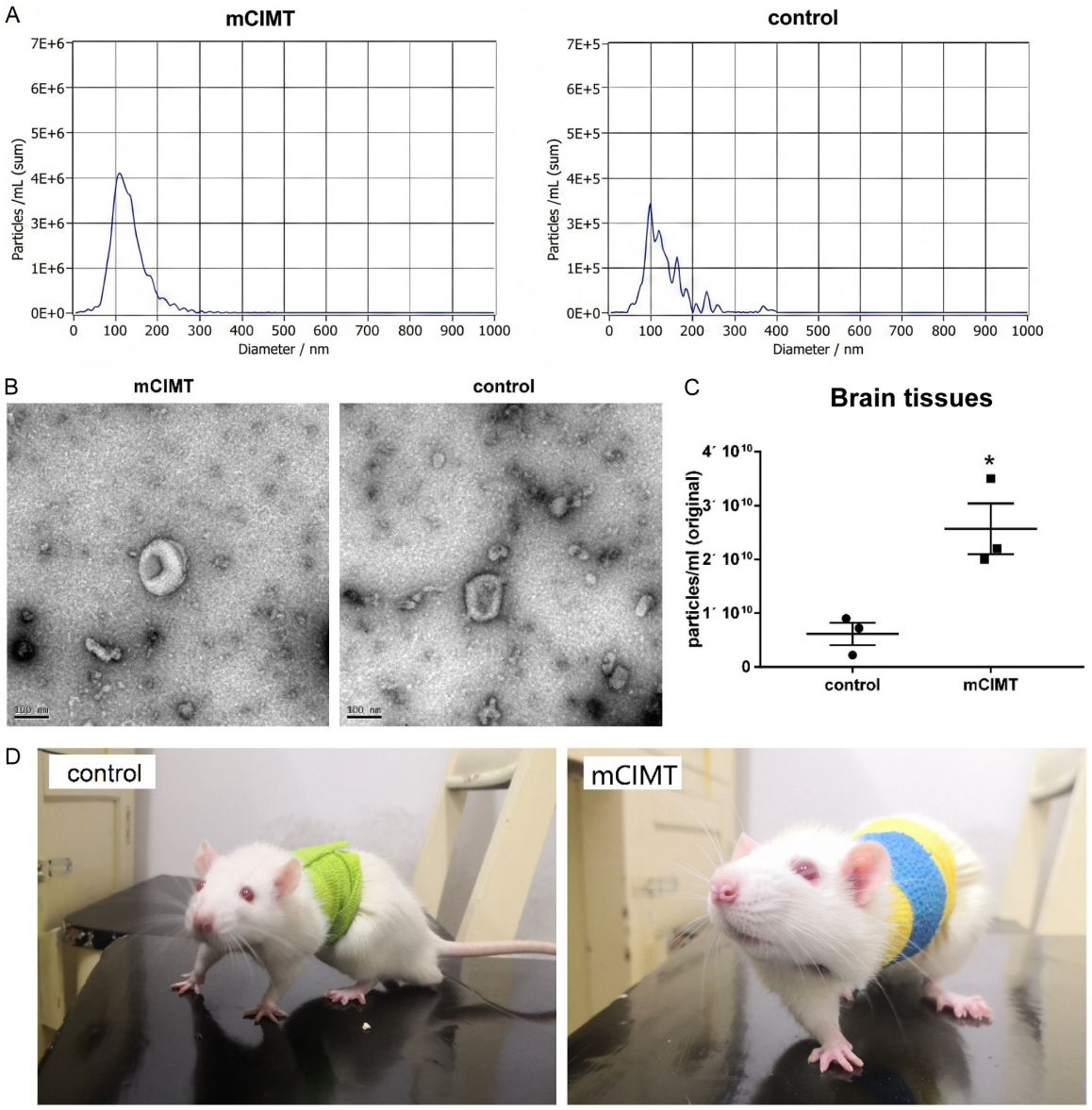

Figure 2. mCIMT increases the concentration of exosomes in brain tissues of MCAO model. A. NTA reveals the peak value of the particle size and the percentage of the peak area. The size of exosomes is generally in the range of 30-200 nm. B. Ultrastructure of the exosomes observed via transmission electron microscopy (80000×). Scale bar=100 nm. C. Concentration of exosomes in the plasma of mCIMT and control groups. D. In the mCIMT group, the unaffected limb (left forelimb) was restrained against the chest using a bandage, while the control group underwent identical chest handling without limb restrain. N=4 animals/group, *P<0.05.

A heatmap illustrates the differences in microRNA expression between the two groups (**Figure 3A**). It provides an overview of the microRNA sequencing results from four samples across the two groups: samples 1 and 2 belong to the control group, while samples 3 and 4 belong to the mCIMT group. Principal component analysis (PCA) and degree distribution were used for dimensionality reduction, identifying key differential microRNAs that play a "hub" role in the dataset (**Figure 3B**). Subsequently, a visual representation was created to display the distribution of these key microRNAs between the two groups (**Figure 3C**). Using TargetScan, a tool for predicting miRNA target genes, the top 30 miRNAs (ranked in descending order by degree) were shown in a bar chart (**Figure 3D**). Additionally, the top 30 target genes (also ranked in descending order by degree) were visualized (**Figure 3E**). The prediction of biologi-

Table 4. Typical microRNAs in the brain tissue exosomes affected by mCIMT

miRNA	Control group (n=4)	mCIMT group (n=4)	Fold change	*p*-value	Regulation
miR-7a-5p	204.26	1438.05	2.815635223	<0.001	Up ↑
miR-450a-5p	53.99	134.76	1.319628212	<0.001	Up ↑
miR-335-5p	153.32	367.88	1.262689342	<0.001	Up ↑
let-7a-5p	6329.98	13024.3	1.040932989	<0.001	Up ↑
miR-125a-3p	15.95	1.6	-3.31741261	<0.001	Down ↓
miR-7b-5p	495.68	0.001	-18.9190495	<0.001	Down ↓

cal targets was based on precise matches between the miRNA seed regions and their target 3'UTRs, prioritizing miRNA-target interactions based on predicted targeting efficiency and conservation. In the pathways observed between two groups, several pathways were specific to the mCIMT group. For example, "MAPK signaling pathways" "G protein signaling pathways" "TGF-b signaling pathways" from Wiki-pathways enrichment analysis (**Figure 3F**).

Histopathological changes were observed in brain tissue after stereotactic injection of exosomes

We administered exosomes and vehicle into the lateral ventricles of MCAO model rats using stereotactic injection on the 7th day following MCAO. The Exo-mCIMT group, Exo-control group, and vehicle group (N=4 per group) underwent histopathological staining of brain tissue on the 21st day post-MCAO. After immunofluorescence staining, the region of interest was the primary motor cortex on the lesioned side of the brain (**Figure 4A**). We observed that the number of VEGF+ cells in the Exo-mCIMT group was significantly more than in the other two groups (P=0.0038 compared to Exo-control, P<0.0001 compared to vehicle), and the VEGF+ cells in the Exo-control group was more than in the vehicle group (P=0.0061) (**Figure 4B**). The MAP2+ in the Exo-mCIMT group was markedly more than in the Exo-control group (P<0.0001) and the vehicle group (P<0.0001) (**Figure 4C**).

Characteristic behavioral gait changes were observed after stereotactic injection of exosomes in rats

We injected exosomes and vehicle into the lateral ventricles of MCAO model rats via stereotactic injection on the 7th day after MCAO. **Figure 5A** shows cartoons of various gait features extracted from the plantar surface of the rats' feet after walking using our equipment for analysis. The Exo-mCIMT group, Exo-control group, and vehicle group (N=9) underwent two behavioral tests on the T1 (14th day) and T2 (21st day) post-MCAO. We found two of the characteristics, max contact intensity and plantar width, were significantly different between the three groups (**Figure 5B**). Compared with T1, the Max contact intensity values of the affected forelimb in the Exo-mCIMT group were significantly greater on T2 (P=0.0263), but not in other two groups (**Figure 5C**). Similarly, compared with T1, the print width values of the affected forelimb in the Exo-mCIMT group (P=0.0135) were significantly greater on T2 (**Figure 5D**).

Discussion and conclusion

The current landscape of stroke rehabilitation emphasizes the importance of innovative therapeutic approaches to enhance recovery. Traditional methods often fall short in promoting significant neural regeneration and functional recovery. Recent studies have begun to explore the role of exosomes and microRNAs in mediating neuroprotective effects and facilitating recovery post-stroke. The findings from this investigation reveal that modified constraint-induced movement therapy (mCIMT) markedly elevates exosome concentrations in both the plasma of stroke patients and the brain tissue of MCAO model rats. This increase in exosome content correlates positively with improved motor function, as evidenced by the FMA-UE. Furthermore, the distinct microRNA expression profiles identified in the exosomes suggest that mCIMT not only enhances exosome release but also modulates the molecular signaling pathways involved in neuronal repair and regeneration. These results underscore the potential of mCIMT as a transformative intervention in stroke rehabilitation, highlighting its role in promoting neural recovery through the upregulation of

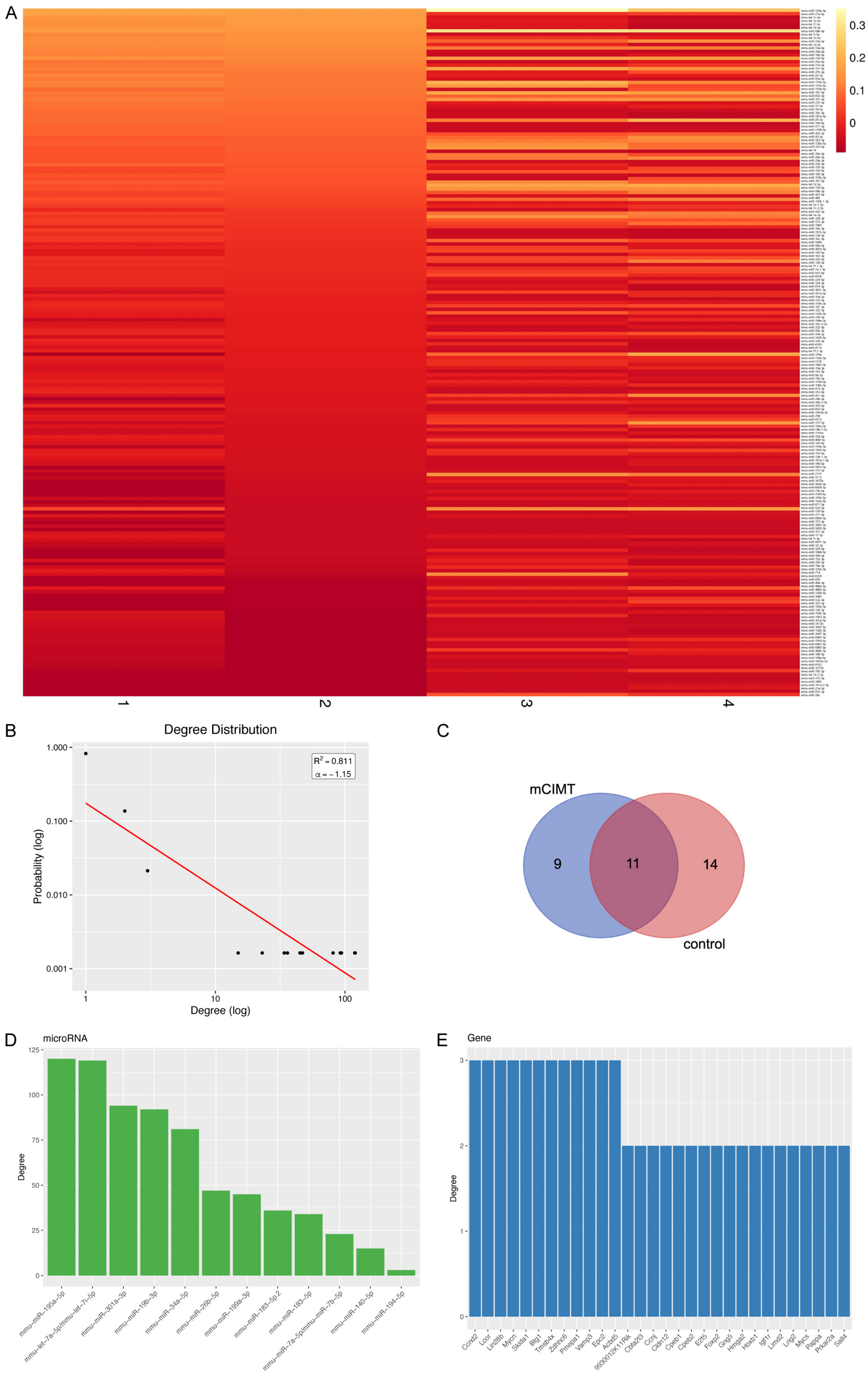
A
1
2
3
4
0.3
0.2
0.1
0
B
Degree Distribution
$R^2 = 0.811$
$\alpha = -1.15$
Probability (log)
Degree (log)
1.000
0.100
0.010
0.001
1
10
100
C
mCIMT
control
9
11
14
D
microRNA
Degree
125
100
75
50
25
0
mmu-miR-195a-5p
mmu-let-7a-5p/mmu-let-7i-5p
mmu-miR-301a-3p
mmu-miR-19b-3p
mmu-miR-34a-5p
mmu-miR-26b-5p
mmu-miR-199a-3p
mmu-miR-183-5p.2
mmu-miR-183-5p
mmu-miR-7a-5p/mmu-miR-7b-5p
mmu-miR-140-5p
mmu-miR-194-5p
E
Gene
Degree
3
2
1
0
Ccnd2
Lcor
Lin28b
Mycn
Skida1
Btg1
Tmsb4x
Zdhhc6
Pmepa1
Vamp3
Epc2
Add3
9930012K11Rik
Cbfa2t3
Ccnj
Cldn12
Cpeb1
Cpeb2
E2f5
Foxp2
Gng5
Hmga2
Hoxb1
Igf1r
Limd2
Lrig2
Mycs
Pappa
Prkar2a
Sall4

Figure 3. MicroRNA sequencing of exosomes derived from brain tissues in the mCIMT and control groups. A. Heatmap showing the relative abundance of exosomal microRNAs (miRNAs) in brain tissue between the two groups after sequencing. B. Degree distribution P(k)P(k), where kk represents the degree. The log-log plot of P(k)P(k) (Y-axis) versus kk (X-axis) is presented. Using the least squares method, the best-fit curve was determined, yielding a residual sum of squares (R2R^2) of 0.811 and an estimated coefficient α\alpha of -1.15. C. Venn diagram illustrating the distribution of differentially expressed miRNAs between the mCIMT and control groups. D. Bar graph depicting the degree of miRNAs, with the X-axis showing the top 30 miRNAs ranked in descending order of degree (i.e., the number of their targets) and the Y-axis representing their degree. E. Bar graph of mRNA (messenger RNA) degrees, with the X-axis displaying the top 30 target genes ranked in descending order of degree (i.e., the number of miRNAs targeting them) and the Y-axis representing their degree. F. WikiPathways, Reactome, and KEGG pathway analyses of the differential target genes identified between the mCIMT and control groups. The Y-axis displays annotated pathway categories, while the X-axis indicates miRNA families with at least one annotated target, with the number of identified targets shown in parentheses. The color of the points represents the adjusted *p*-value (false discovery rate, FDR), and the size of the points indicates the gene ratio (i.e., the number of annotated miRNA targets in each category divided by the total number of identified targets shown in parentheses).

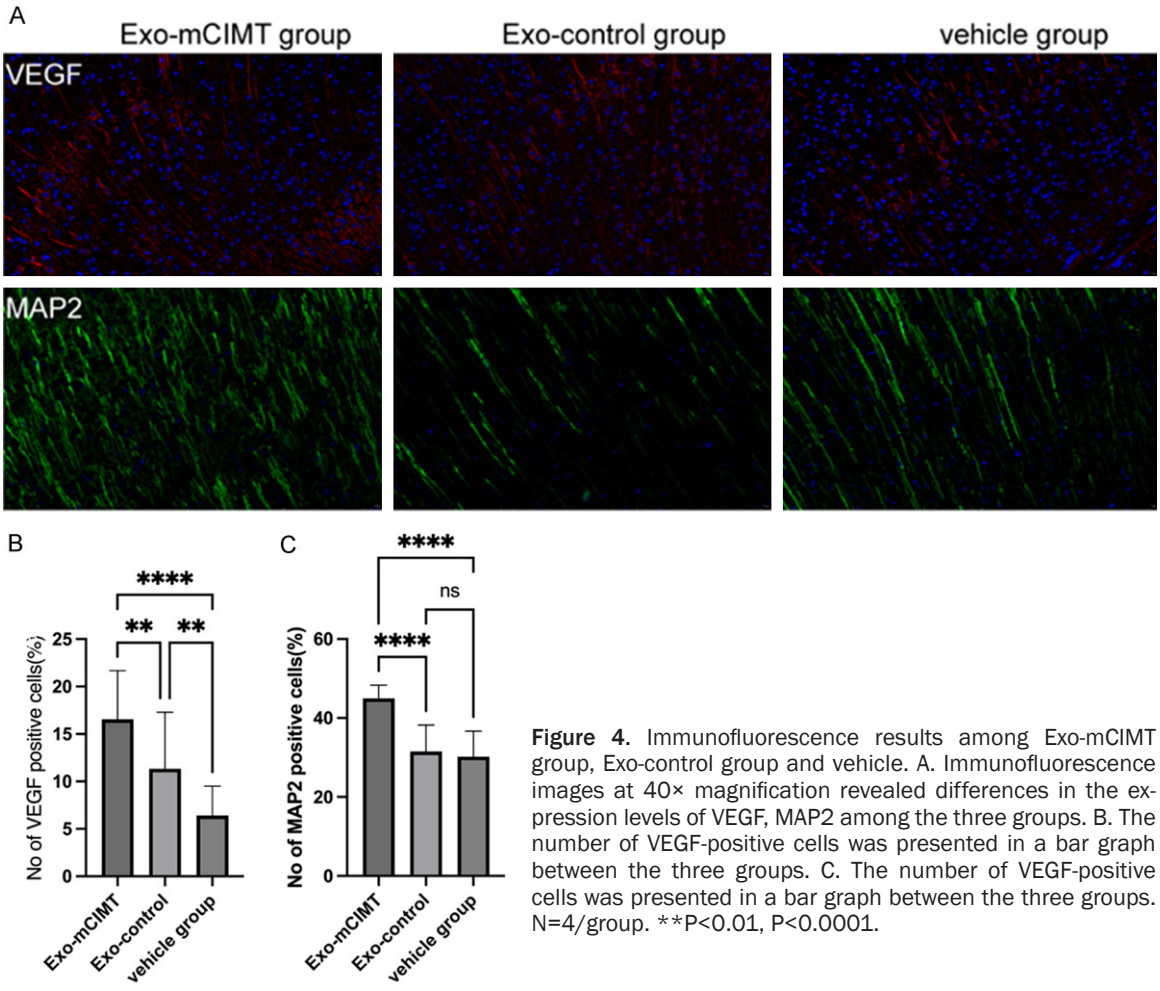

Figure 4. Immunofluorescence results among Exo-mCIMT group, Exo-control group and vehicle. A. Immunofluorescence images at 40× magnification revealed differences in the expression levels of VEGF, MAP2 among the three groups. B. The number of VEGF-positive cells was presented in a bar graph between the three groups. C. The number of VEGF-positive cells was presented in a bar graph between the three groups. N=4/group. **P<0.01, P<0.0001.

exosomal and microRNA activity. The implications of this research extend beyond immediate clinical applications, paving the way for future studies aimed at elucidating the underlying mechanisms of exosome-mediated neuroprotection and their therapeutic potential in stroke recovery.

Forced exercise, particularly CIMT and its modified versions, is a rehabilitation approach aimed at promoting post-stroke functional recovery. It primarily involves restricting the unaffected limb's activity to compel the affected limb to engage in motor training, thereby reshaping brain functional connectivity and improving motor performance. The increased exosomal activity may be directly linked to improved motor function as evidenced by the correlation with the Fugl-Meyer Motor Function Assessment Upper Extremity (FMA-UE) scores (R^2=0.428). The increased exosomal diameter in the mCIMT group may reflect a higher loading of therapeutic microRNAs, which could be pivotal in enhancing synaptic plasticity and neurogenesis. Moreover, the distinct expression profiles of microRNAs identified through sequencing highlight the specificity of mCIMT in modulating molecular pathways associated with neural recovery.

Many studies have shown that CIMT significantly enhances motor function in MCAO model rats, such as forelimb grip strength and gait analysis parameters [8, 34]. Research also indicates that CIMT facilitates motor recovery independently of cognitive improvements [12]. The efficacy of CIMT depends on the timing of intervention, with early treatment being considered optimal for maximizing neurological recovery [35]. CIMT exerts its effects by increasing the number and strength of synaptic connections, thereby enhancing neural network inte-

A

B

		P Value
Stand	(s)	NA
Max Contact Area	(cm^2)	NA
Max Contact Intensity	Mean	***
Print Length	(cm)	NA
Print Width	(cm)	**
Print Area	(cm^2)	NA
Max Intensity	Mean	NA
Min Intensity	Mean	NA
Mean Intensity	Mean	NA
Swing	(s)	NA
Swing Speed	(cm/s)	NA
Stride Length	(cm)	NA
Step Cycle	(s)	NA
Duty Cycle	(%)	NA
Single Stance	(s)	NA
Initial Dual Stance	(s)	NA
Terminal Dual Stance	(s)	NA
Body Speed	(cm/s)	NA
Body Speed Variation	(%)	NA

C

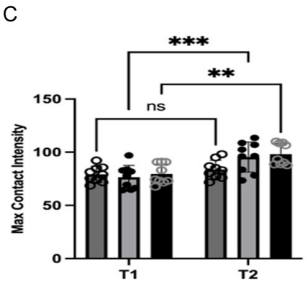

D

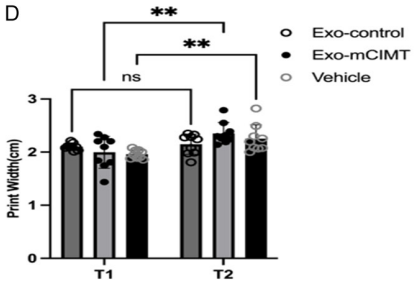

Figure 5. Behavioural evaluation of rats in Exo-mCIMT group, Exo-control group and vehicle. A. Cartoon of various features of gait, extracted from the plantar surface of the foot after walking in rats using our equipment for analysis. B. Walking characteristics data extracted by the device and managed by the upper limb function. Two of the characteristics, max contact intensity and plantar width, were significantly different between the three groups. C. A two-by-two analysis revealed that the characteristic indicator of max contact intensity, only in the mCIMT group, was significantly improved before and after the different time points. There was no difference between the other two groups. D. The characteristic indicator of plantar width, only the mCIMT group, was significantly improved before and after the different time points. There was no difference between the other two groups. N=9/group, **P<0.01. ***P<0.001.

gration [7, 34, 36]. CIMT promotes neural stem cell proliferation and differentiation in ischemic brain regions, such as the hippocampus and cortex, aiding the integration of newly formed neurons [37-39]. CIMT likely modulates the neurovascular unit, fostering vascular growth and blood flow restoration in ischemic regions [10, 38]. CIMT mitigates neuronal apoptosis and creates a favorable environment for neuronal survival1. Key molecules involved include BDNF (brain-derived neurotrophic factor) [10, 16-18], which enhances synaptic plasticity and neuronal survival, and VEGF (vascular endothelial growth factor) [10, 38], which supports endothelial and vascular function. Pathways implicated include the Nogo-A-RhoA-ROCK [37], P-JNK/JNK2 pathway [8], and ROCK signaling [35]. In this study We discovered that mCIMT promotes the release of exosomes, potentially contributing to functional recovery in stroke patients. To validate this hypothesis, we established a stroke model using the MCAO method. Exosomes were extracted from brain tissue and stereotactically injected into MCAO model rats, which subsequently demonstrated improved neurobehavioral outcomes and enhanced brain tissue repair.

This study hypothesizes that CIMT promotes neural repair by increasing the concentration of exosomes in serum, particularly those carrying neuroprotective miRNAs. Through this research, we demonstrated that CIMT modulates the expression of specific miRNAs, thereby influencing the neuro-environmental balance. Moreover, the elevated exosome concentrations in the brain tissue of rats subjected to mCIMT further support the notion that molecular changes induced by this therapy can lead to phenotypic improvements. The distinct microRNA expres-

sion profiles identified in the exosomes from the mCIMT group suggest that these molecules may play a pivotal role in modulating neuronal activity and promoting recovery after ischemic injury. The KEGG enrichment analysis highlights specific signaling pathways that are likely influenced by the microRNAs, providing insights into the molecular mechanisms underlying the observed phenotypic changes.

Exosomes play roles in central nervous system processes, including synaptic plasticity, neuronal stress responses, intercellular communication, and neurogenesis. The biological functions of exosomes are often related to their contents, such as microRNAs. MicroRNAs, short noncoding RNA molecules, are crucial for neuronal development. Their most common function is to target and negatively regulate mRNAs, thus mediating their degradation [40-42]. Research has shown that the neuroprotective effect of cerebral ischaemic preconditioning may be related to astrocyte secretion of exosomes enriched with microRNA-92b [43]. Moderate exercise may provide protection against the acute and chronic phases of cerebral ischaemic injury by inducing the release of circulating endothelial progenitor cell-derived exosomes [44]. Plasma exosomes isolated from exercised rats have been shown to exert significant protective effects against myocardial ischaemia/reperfusion injury. Exercise training or laminar shear stress directly increases the synthesis of miR-342-5p in endothelial cells, which inhibits hypoxia/reoxygenation-induced apoptosis in cardiomyocytes by targeting the regulation of Caspase 9 and JNK2 [45]. Therefore, exosomes and their microRNA contents are integral to various physiological and pathological processes in the central nervous system, with potential therapeutic applications in conditions such as cerebral ischaemia and myocardial injury. Our data collectively suggests that mCIMT not only enhances exosome release but also alters the microRNA landscape, which in turn contributes to improved motor function. This molecular-phenotype relationship emphasizes the importance of exosomes and their cargo in mediating the therapeutic effects of mCIMT, paving the way for future research aimed at harnessing these molecular entities for enhanced stroke recovery strategies. Extensive studies have demonstrated that exosome-enriched miRNAs can regulate apoptosis, inflammatory responses, and oxidative stress, promoting neuronal survival and functional recovery. For instance, miR-21 [46] and miR-124 [47] suppress the expression of apoptosis-related genes, protecting neurons from ischemic injury. Additionally, exosomes can enhance neuronal ischemic tolerance by regulating the release of neuroprotective factors, improving prognosis in ischemic stroke [48]. miRNAs like miR-146a [49] promote neural stem cell proliferation and differentiation, bolstering neuroregeneration. Exosome-carried miRNAs suppress apoptotic signaling pathways, safeguarding neurons from damage, facilitating functional recovery, thereby offering novel therapeutic avenues for ischemic stroke. miR-155 modulates microglial activation states, reducing excessive inflammation to protect neurons [50, 51]. Furthermore, miR-126 has been shown to promote endothelial cell migration and angiogenesis, enhancing post-ischemic blood flow [52]. Exosomal miRNAs also influence immune cell function, regulate fibroblasts and other support cells, and promote tissue repair and regeneration [48, 53].

Moreover, the distinct microRNA expression profiles highlighted by sequencing further reinforce the mCIMT-neuroprotection paradigm, indicating that mCIMT not only alters exosome quantity but also influences the specific microRNA content and associated pathways. The KEGG enrichment analysis revealed the activation of signaling pathways that play pivotal roles in neuronal repair and neuroprotection, thus delineating a clear mechanistic link between the therapeutic intervention and phenotypic recovery. This integrated understanding emphasizes the significance of mCIMT in rewiring the molecular landscape following ischemic injury, thereby underscoring the treatment's potential to improve functional outcomes via exosome-mediated molecular communication.

The limitations of this investigation warrant careful consideration, it is recommended that future confirmatory studies appropriately increase the sample size based on the above principles and include an additional 10-20% to account for loss to follow-up and sample quality control failures. The relatively small sample size of human participants, with only 16 stroke patients, may restrict the generalizability of

the findings. Additionally, the lack of long-term follow-up for assessing sustained effects of mCIMT on functional recovery poses another challenge. Another limitation of this study is the absence of a healthy control group for comparative analysis of serum inflammatory cytokines and exosome characteristics. While this design aligns with the primary objective of evaluating the relative changes induced by mCIMT within stroke subjects and animal models, rather than establishing population-based normative values, it restricts direct interpretation of how these parameters differ from non-stroke conditions. Future studies would benefit from incorporating age- and sex-matched healthy controls to provide a foundational reference, allowing clearer discrimination between disease-specific alterations and therapy-associated modifications. Furthermore, the reliance on animal models may not fully replicate the complexities of human stroke recovery, necessitating further studies to validate these observations in diverse populations and extended timelines.

To conclude, mCIMT enhances neural recovery post-stroke by elevating exosome concentrations and microRNA profiles, as evidenced through significant evaluations of plasma and brain tissue samples from stroke patients and MCAO model rats. The correlation between increased exosome content and improved motor function underscores mCIMT's potential as an influential rehabilitation strategy. Furthermore, distinct microRNA expression patterns and signaling pathways illuminate the mechanistic role of exosomes in promoting neuronal activity and recovery after cerebral ischemic injury, establishing mCIMT as a promising therapeutic approach in stroke rehabilitation.

Acknowledgements

We thank the staff of the Department of Rehabilitation Medicine and the Department of Clinical Research and Data Management for their participation in this research. This work was supported by the National High-Level Hospital Clinical Research Funding (2025-NHLHCRF-PY-41), the National Natural Science Foundation of China (82102654), the Beijing Natural Science Foundation (2024BZR-7242126), and the 2023 Beijing Municipal Clinical Key Specialty Construction Project.

Disclosure of conflict of interest

None.

Address correspondence to: Dr. Shan Jiang, Department of Rehabilitation Medicine, China-Japan Friendship Hospital, Yinghuayuan East St. Hepingli, Chaoyang District, Beijing 100029, China. Tel: +86-18610335283; E-mail: landjiang@126.com

References

[1] de Azevedo JA, Barbosa FDS, Seixas VM, da Silva Scipioni KRD, Sampaio PYS, da Cruz DMC, Piscitelli D, Chui KK and de Freitas Zanona A. Effects of constraint-induced movement therapy on activity and participation after a stroke: systematic review and meta-analysis. Front Hum Neurosci 2022; 16: 987061.

[2] Tedla JS, Gular K, Reddy RS, de Sa Ferreira A, Rodrigues EC, Kakaraparthi VN, Gyer G, Sangadala DR, Qasheesh M, Kovela RK and Nambi G. Effectiveness of constraint-induced movement therapy (CIMT) on balance and functional mobility in the stroke population: a systematic review and meta-analysis. Healthcare (Basel) 2022; 10: 459.

[3] Palomo-Carrion R, Romay-Barrero H, Romero-Galisteo RP, Pinero-Pinto E, Lopez-Munoz P and Martinez-Galan I. Modified constraint-induced movement therapy at home-is it possible? Families and children's experience. Children (Basel) 2020; 7: 248.

[4] Sicari M, Longhi M, D'Angelo G, Boetto V, Lavorato A, Cocchini L, Beatrici M, Battiston B, Garbossa D, Massazza G and Titolo P. Modified constraint induced movement therapy in children with obstetric brachial plexus palsy: a systematic review. Eur J Phys Rehabil Med 2022; 58: 43-50.

[5] Fleet A, Page SJ, MacKay-Lyons M and Boe SG. Modified constraint-induced movement therapy for upper extremity recovery post stroke: what is the evidence? Top Stroke Rehabil 2014; 21: 319-331.

[6] Shi YX, Tian JH, Yang KH and Zhao Y. Modified constraint-induced movement therapy versus traditional rehabilitation in patients with upper-extremity dysfunction after stroke: a systematic review and meta-analysis. Arch Phys Med Rehabil 2011; 92: 972-982.

[7] Liu P, Li C, Zhang B, Zhang Z, Gao B, Liu Y, Wang Y, Hua Y, Hu J, Qiu X and Bai Y. Constraint induced movement therapy promotes contralesional-oriented structural and bihemispheric functional neuroplasticity after stroke. Brain Res Bull 2019; 150: 201-206.

[8] Hu J, Li C, Hua Y, Zhang B, Gao BY, Liu PL, Sun LM, Lu RR, Wang YY and Bai YL. Constrained-induced movement therapy promotes motor function recovery by enhancing the remodeling of ipsilesional corticospinal tract in rats after stroke. Brain Res 2019; 1708: 27-35.

[9] Kerr AL. Contralesional plasticity following constraint-induced movement therapy benefits outcome: contributions of the intact hemisphere to functional recovery. Rev Neurosci 2021; 33: 269-283.
[10] Wang D, Li L, Zhang Q, Liang Z, Huang L, He C and Wei Q. Combination of electroacupuncture and constraint-induced movement therapy enhances functional recovery after ischemic stroke in rats. J Mol Neurosci 2021; 71: 2116-2125.
[11] Abdullahi A, Truijen S and Saeys W. Neurobiology of recovery of motor function after stroke: the central nervous system biomarker effects of constraint-induced movement therapy. Neural Plast 2020; 2020: 9484298.
[12] Gao BY, Xu DS, Liu PL, Li C, Du L, Hua Y, Hu J, Hou JY and Bai YL. Modified constraint-induced movement therapy alters synaptic plasticity of rat contralateral hippocampus following middle cerebral artery occlusion. Neural Regen Res 2020; 15: 1045-1057.
[13] Liu XH, Bi HY, Cao J, Ren S and Yue SW. Early constraint-induced movement therapy affects behavior and neuronal plasticity in ischemia-injured rat brains. Neural Regen Res 2019; 14: 775-782.
[14] Alcantara CC, Garcia-Salazar LF, Silva-Couto MA, Santos GL, Reisman DS and Russo TL. Post-stroke BDNF concentration changes following physical exercise: a systematic review. Front Neurol 2018; 9: 637.
[15] Shiner CT, Pierce KD, Thompson-Butel AG, Trinh T, Schofield PR and McNulty PA. BDNF genotype interacts with motor function to influence rehabilitation responsiveness poststroke. Front Neurol 2016; 7: 69.
[16] Ishida A, Misumi S, Ueda Y, Shimizu Y, Cha-Gyun J, Tamakoshi K, Ishida K and Hida H. Early constraint-induced movement therapy promotes functional recovery and neuronal plasticity in a subcortical hemorrhage model rat. Behav Brain Res 2015; 284: 158-166.
[17] Livingston-Thomas JM, McGuire EP, Doucette TA and Tasker RA. Voluntary forced use of the impaired limb following stroke facilitates functional recovery in the rat. Behav Brain Res 2014; 261: 210-219.
[18] Livingston-Thomas JM, Hume AW, Doucette TA and Tasker RA. A novel approach to induction and rehabilitation of deficits in forelimb function in a rat model of ischemic stroke. Acta Pharmacol Sin 2013; 34: 104-112.
[19] Colvett I, Saternos H, Coughlan C, Vielle A and Ledreux A. Extracellular vesicles from the CNS play pivotal roles in neuroprotection and neurodegeneration: lessons from in vitro experiments. Extracell Vesicles Circ Nucl Acids 2023; 4: 72-89.
[20] Ramirez SH, Andrews AM, Paul D and Pachter JS. Extracellular vesicles: mediators and biomarkers of pathology along CNS barriers. Fluids Barriers CNS 2018; 15: 19.
[21] Hirshman BR, Kras RT, Akers JC, Carter BS and Chen CC. Extracellular vesicles in molecular diagnostics: an overview with a focus on CNS diseases. Adv Clin Chem 2016; 76: 37-53.
[22] Tang X, Ren Y, Zeng W, Feng X, He M, Lv Y, Li Y and He Y. MicroRNA-based interventions in aberrant cell cycle diseases: Therapeutic strategies for cancers, central nervous system disorders and comorbidities. Biomed Pharmacother 2024; 177: 116979.
[23] Zhang L, Mao L and Wang H. The neuroprotection effects of exosome in central nervous system injuries: a new target for therapeutic intervention. Mol Neurobiol 2022; 59: 7152-7169.
[24] Yu Y, Hou K, Ji T, Wang X, Liu Y, Zheng Y, Xu J, Hou Y and Chi G. The role of exosomal microRNAs in central nervous system diseases. Mol Cell Biochem 2021; 476: 2111-2124.
[25] Xin H, Li Y and Chopp M. Exosomes/miRNAs as mediating cell-based therapy of stroke. Front Cell Neurosci 2014; 8: 377.
[26] Otero-Ortega L, Gomez de Frutos MC, Laso-Garcia F, Rodriguez-Frutos B, Medina-Gutierrez E, Lopez JA, Vazquez J, Diez-Tejedor E and Gutierrez-Fernandez M. Exosomes promote restoration after an experimental animal model of intracerebral hemorrhage. J Cereb Blood Flow Metab 2018; 38: 767-779.
[27] Pascual M, Ibanez F and Guerri C. Exosomes as mediators of neuron-glia communication in neuroinflammation. Neural Regen Res 2020; 15: 796-801.
[28] Xiao B, Chai Y, Lv S, Ye M, Wu M, Xie L, Fan Y, Zhu X and Gao Z. Endothelial cell-derived exosomes protect SH-SY5Y nerve cells against ischemia/reperfusion injury. Int J Mol Med 2017; 40: 1201-1209.
[29] Xin H, Li Y, Cui Y, Yang JJ, Zhang ZG and Chopp M. Systemic administration of exosomes released from mesenchymal stromal cells promote functional recovery and neurovascular plasticity after stroke in rats. J Cereb Blood Flow Metab 2013; 33: 1711-1715.
[30] Xin H, Li Y, Liu Z, Wang X, Shang X, Cui Y, Zhang ZG and Chopp M. MiR-133b promotes neural plasticity and functional recovery after treatment of stroke with multipotent mesenchymal stromal cells in rats via transfer of exosome-enriched extracellular particles. Stem Cells 2013; 31: 2737-2746.
[31] Xin H, Li Y, Buller B, Katakowski M, Zhang Y, Wang X, Shang X, Zhang ZG and Chopp M. Exosome-mediated transfer of miR-133b from multipotent mesenchymal stromal cells to neural cells contributes to neurite outgrowth. Stem Cells 2012; 30: 1556-1564.

[32] Hurwitz SN, Olcese JM and Meckes DG Jr. Extraction of extracellular vesicles from whole tissue. J Vis Exp 2019; 7: 10.3791/59143.
[33] Vella LJ, Scicluna BJ, Cheng L, Bawden EG, Masters CL, Ang CS, Willamson N, McLean C, Barnham KJ and Hill AF. A rigorous method to enrich for exosomes from brain tissue. J Extracell Vesicles 2017; 6: 1348885.
[34] Hu J, Li C, Hua Y, Liu P, Gao B, Wang Y and Bai Y. Constraint-induced movement therapy improves functional recovery after ischemic stroke and its impacts on synaptic plasticity in sensorimotor cortex and hippocampus. Brain Res Bull 2020; 160: 8-23.
[35] Liu YH, Zhao Y, Huang FZ, Chen YH, Wang HX, Bonney E and Liu BQ. Combination of early constraint-induced movement therapy and fasudil enhances motor recovery after ischemic stroke in rats. Int J Neurosci 2016; 126: 168-173.
[36] Zhao S, Zhao M, Xiao T, Jolkkonen J and Zhao C. Constraint-induced movement therapy overcomes the intrinsic axonal growth-inhibitory signals in stroke rats. Stroke 2013; 44: 1698-1705.
[37] Zhai Z and Guo Y. Combination of constraint-induced movement therapy with fasudil amplifies neurogenesis after focal cerebral ischemia/reperfusion in rats. Int J Neurosci 2022; 132: 1254-1260.
[38] Li C, Zhang B, Zhu Y, Li Y, Liu P, Gao B, Tian S, Du L and Bai Y. Post-stroke constraint-induced movement therapy increases functional recovery, angiogenesis, and neurogenesis with enhanced expression of HIF-1α and VEGF. Curr Neurovasc Res 2017; 14: 368-377.
[39] Zhao C, Wang J, Zhao S and Nie Y. Constraint-induced movement therapy enhanced neurogenesis and behavioral recovery after stroke in adult rats. Tohoku J Exp Med 2009; 218: 301-308.
[40] Bian S, Xu TL and Sun T. Tuning the cell fate of neurons and glia by microRNAs. Curr Opin Neurobiol 2013; 23: 928-934.
[41] Fineberg SK, Kosik KS and Davidson BL. MicroRNAs potentiate neural development. Neuron 2009; 64: 303-309.
[42] Shi Y, Zhao X, Hsieh J, Wichterle H, Impey S, Banerjee S, Neveu P and Kosik KS. MicroRNA regulation of neural stem cells and neurogenesis. J Neurosci 2010; 30: 14931-14936.
[43] Xu L, Cao H, Xie Y, Zhang Y, Du M, Xu X, Ye R and Liu X. Exosome-shuttled miR-92b-3p from ischemic preconditioned astrocytes protects neurons against oxygen and glucose deprivation. Brain Res 2019; 1717: 66-73.
[44] Wang J, Liu H, Chen S, Zhang W, Chen Y and Yang Y. Moderate exercise has beneficial effects on mouse ischemic stroke by enhancing the functions of circulating endothelial progenitor cell-derived exosomes. Exp Neurol 2020; 330: 113325.
[45] Hou Z, Qin X, Hu Y, Zhang X, Li G, Wu J, Li J, Sha J, Chen J, Xia J, Wang L and Gao F. Longterm exercise-derived exosomal miR-342-5p: a novel exerkine for cardioprotection. Circ Res 2019; 124: 1386-1400.
[46] Liu C, Yin T, Zhang M, Li Z, Xu B, Lv H, Wang P, Wang J, Hao J and Zhang L. Function of miR-21-5p derived from ADSCs-exos on the neuroinflammation after cerebral ischemia. J Stroke Cerebrovasc Dis 2024; 33: 107779.
[47] Zhu Y, Zhao X, Liu R, Yang D and Ge G. Effect of oxygen-glucose deprivation of microglia-derived exosomes on hippocampal neurons: a study on miR-124 and inflammatory cytokines. J Mol Histol 2024; 55: 349-357.
[48] Nagase T, Kin K and Yasuhara T. Targeting neurogenesis in seeking novel treatments for ischemic stroke. Biomedicines 2023; 11: 2773.
[49] Zhang Z, Zou X, Zhang R, Xie Y, Feng Z, Li F, Han J, Sun H, Ouyang Q, Hua S, Lv B, Hua T, Liu Z, Cai Y, Zou Y, Tang Y and Jiang X. Human umbilical cord mesenchymal stem cell-derived exosomal miR-146a-5p reduces microglial-mediated neuroinflammation via suppression of the IRAK1/TRAF6 signaling pathway after ischemic stroke. Aging (Albany NY) 2021; 13: 3060-3079.
[50] Otsu Y, Hatakeyama M, Kanayama T, Akiyama N, Ninomiya I, Omae K, Kato T, Onodera O, Fukushima M, Shimohata T and Kanazawa M. Oxygen-glucose deprived peripheral blood mononuclear cells protect against ischemic stroke. Neurotherapeutics 2023; 20: 1369-1387.
[51] Li JJ, Wang B, Kodali MC, Chen C, Kim E, Patters BJ, Lan L, Kumar S, Wang X, Yue J and Liao FF. In vivo evidence for the contribution of peripheral circulating inflammatory exosomes to neuroinflammation. J Neuroinflammation 2018; 15: 8.
[52] Venkat P, Cui C, Chopp M, Zacharek A, Wang F, Landschoot-Ward J, Shen Y and Chen J. MiR-126 mediates brain endothelial cell exosome treatment-induced neurorestorative effects after stroke in Type 2 diabetes mellitus mice. Stroke 2019; 50: 2865-2874.
[53] Wang X, Fu CH, Zhu X, Liu J, Gong X, Pan Q and Ma X. Exosomes and exosomal microRNAs in age-associated stroke. Curr Vasc Pharmacol 2021; 19: 587-600.